Petroleum Technology Development Journal

Investigation of the effect of reservoir internal structure on waterflood performance: Case Study of Reservoir X

By

Ogbeiwi, Precious* Aladeitan, Yetunde M* Udebhulu Dickson Okhira*

ABSTRACT

Waterflooding is the dominant secondary oil recovery method due to the relative ease of finding water for injection and its ability to move through oil-bearing formations, displacing oil in the process. However, the method is plagued with numerous problems. Globally, oil reservoirs which are waterflooded are usually associated with significant volumes of shale which create discontinuities within the reservoir units thus dividing them into several flow units. Hence, to accurately predict the performance of a waterflooding scheme, the effects of the presence of these flow barriers/discontinuities caused by sand-shale sequence, reservoir heterogeneity and anisotropy on the process, must first be assessed. This study was aimed at investigating the effects of sand discontinuities, reservoir heterogeneity (measured using the Dysktra-Parsons Coefficient) and variations in vertical-to-horizontal permeability on drainage and injection pattern of a reservoir. The geostatistical tool, SGEMS, was used to build static models of reservoir properties of interest. The resulting geostatistical models were then used to build dynamic reservoir models which were predictive tools in the waterflood simulations carried out using the Coates Engineering Sensor 6.4 reservoir simulator. The results showed that variations in kV/kH ratio, as well as reservoir lateral and vertical heterogeneity, play a significant role in the performance of waterflooding.

Keywords: Waterflooding, oil recovery, static reservoir models, reservoir heterogeneity, permeability.

INTRODUCTION

Because of the decreasing discovery of new oil and gas fields over the years, it has become imperative to produce existing mature oil field more efficiently and economically, using secondary and tertiary oil recovery mechanisms[1]. According to Craig[2], waterflooding is one of the most widely used secondary oil recovery means after the exhaustion of the primary depletion energy of a reservoir, and it is known to be responsible for high oil production rates in mature oil fields of the U.S and Canada. It basically involves pumping water through an injection well into the reservoir which then forces itself through the pore spaces of the reservoir rock and sweeps the oil towards another set of wells known as producers. This leads to an increase in the total oil production from the reservoir. However, the quantity of water in the produced fluids steadily increases. Meshioye *et al*.[3] ascertained that on the average, this process can lead to the recovery of about one-third of the original oil in place (OOIP), leaving behind about two-thirds. As discussed

* Department of Petroleum Engineering, African University of Science and Technology Abuja
Email yetty76@yahoo.com

[1]Nwaozo J., (2006), Dynamic Optimization of a Water Flood Reservoir, M Sc. Thesis, University of Oklahoma Graduate College, Norman, Oklahoma, USA.

[2]Craig F.F. (1971), The Reservoir Engineering Aspects of Waterflooding. Society of Petroleum Engineers, New York, Dallas.

[3]Meshioye O., Mackay E., and Chukuwezi M. (2010), Optimization of Waterflooding Using Smart Well Technology. Paper SPE 136996 presented at the 34th Annual SPE International Conference and Exhibition held in Tinapa – Calabar, Nigeria, 31 July.

by Asadollahi[4], the popularity of water injection is mainly due to water availability, mobility, displacement efficiency and ease of injection.

Even with its numerous advantages, like any other process, waterflood still has lots of challenges. Handyside *et al.*[5] noted that poor sweep efficiency and low contact factor are common problems that plague waterflooding. The contact factor is determined by improper displacement in a direction orthogonal to the reservoir strata. In reservoirs with lateral heterogeneity, or those in which bedding planes exhibit anisotropy, poor areal displacement efficiency is common. This means large areas are left with high oil saturation for a given economically acceptable watercut in the production wells.

According to Awejori *et al.*[6], large hydrocarbon volumes are found in reservoir systems associated with high shale volumes. These high shale volumes create heterogeneities and discontinuities within the reservoir units and this causes the reservoir to be divided into several flow units. The presence of flow barriers caused by these shales and variations in directional permeability across the reservoir strongly affects the drainage patterns and the sweep efficiency of water injection processes.

Therefore, to accurately estimate the efficiency of a waterflooding process, an assessment of the impact of sand discontinuities or connectivities in these reservoirs is required for realistic performance predictions of the schemes and estimation of associated confidence limits. This is particularly important during the pre-development stage when major investment decisions are to be made based on a limited number of exploration wells, since these reservoir systems are composed of various genetic reservoir units ranging from clean channel lag and storey axis sands, with a high net-to-gross to thin-bedded levee over-bank deposits containing lower sand fractions.

Several authors have presented methodologies involving the use of geostatistical and/or dynamic reservoir simulation as predictive tools for reservoir management; some of them are presented below:

Akingbade *et al.*[7] sought to identify and reduce uncertainty in the depositional architecture of the Bonga field reservoir in the offshore Niger Delta adopting a holistic approach involving the use of loop stratigraphy interpretation, as well as detailed static and dynamic modeling techniques. Their results showed that integrating static and dynamic modeling provides a better way of understanding reservoirs by eliminating scenarios that do not honor all the data available.

Abbaszadeh *et al.*[8] presented a method for an integrated geostatistical reservoir characterization of the Chicontepec field in Mexico, using the multivariate multi-Gaussian technique to integrate data sources and scales. The resulting geostatistical models were then calibrated to available production data, and used as predictive tools for a CO_2-EOR process.

[4]Asadollahi M., (2012). Waterflooding Optimization for Improved Reservoir Management, Ph.D. dissertation, Norwegian University of Science and Technology (NTNU), Trondheim, Norway.
[5]Handyside D. O., Karaoguz O.K., Deskin R.H. and Mattson G.A., (1992), A Practical Application of Stochastic Modeling Techniques for Turbidite Reservoirs. Paper SPE 24892 presented at the 67th Annual Technical Conference and Exhibition of the Society of Petroleum Engineers held in Washington, DC, October 4-7.
[6]Awejori G.A (2010), Integrated Petrophysical Evaluation of Turbiditic Sands in Niger Delta Basin, MSc. Thesis, Unpublished, AUST, 23rd December.
[7]Akingbade, D., Umurhohwo, J., Effiom, O., Pirmez, C. and Weaver, S. (2011), An Integrated Approach to Identifying and Reducing Reservoir Uncertainties in a Turbidite Deep Water Environment. SPE 150740 presented at the Nigeria Annual International Conference and Exhibition held in Abuja, Nigeria, 30 July–3 August.
[8]Abbaszadeh, M., Ohno, K., Okano, H. and Morales, J. (2008), Reservoir Characterization and CO_2-EOR Injection Studies in Chicontepec Turbidite Reservoirs, Mexico. Paper IPTC 12637 presented at the International Petroleum Technology Conference held in Kuala Lumpur, Malaysia, 3–5 December.

Spath *et al.*[9] studied waterflood optimization using a combined geostatistical 3D streamline approach. They used a combination of stochastic reservoir description techniques and streamline simulation to optimize volumetric sweep efficiency in a mature West Texas waterflood. An IMPES, finite-difference scheme was then used to validate the results obtained. Their results showed that the combination of multiple realization property distribution with an efficient streamlined model is a much better alternative to the traditional, finite-difference approach.

This study was aimed at investigating the effects of sand discontinuities, reservoir heterogeneity (measured using the Dysktra-Parsons Coefficient) and variations in vertical-to-horizontal permeability on drainage and injection pattern of a reservoir. The geostatistical tool, SGEMS, was used to build static models of reservoir properties of interest. The resulting geostatistical models were then used to build dynamic reservoir models which were predictive tools in the waterflood simulations carried out using the Coates Engineering Sensor 6.4 reservoir simulator.

METHODOLOGY

This research involved the evaluation of the effect of internal sand distribution on the performance of waterflooding. The study was conducted using data obtained from Reservoir X located in the deep offshore of the Gulf of Mexico. The scope included an assessment of the impact of sand discontinuities or connectivities in turbidite reservoirs using directional permeability variations across the reservoir as well as flow barriers due to shale presence on the drainage and injection patterns of hydrocarbon-bearing petroleum containing rocks. The impact of reservoir heterogeneity (measured using Dykstra-Parsons coefficient) on reservoir/waterflood performance was also analyzed. The scope of this research did not include creating the actual development and production strategy that can be implemented on the reservoir of interest.

The tools used in this study include: The Stanford Geostatistical Modeling Software (SGEMS), and Coates Engineering Sensor 6K. SGEMS was used to create geostatistical models of reservoir properties distributions. These properties included reservoir lithofacies, net-to-gross ratio, shale volume, porosity and permeability. Special emphasis was given to data integration from all available sources so as to constrain computed petrophysical values as well as generate fine-scale property distributions within the reservoirs. The resulting geostatistical models were then used to build various dynamic reservoir models which were predictive tools in the waterflood simulations. Coates Engineering Sensor 6K was used in performing simulations for the different waterflood scenarios analyzed. The simulation results were analyzed by evaluating trends of field average reservoir pressure, oil production rate, cumulative oil production and field water-cut over time for several scenarios of waterflood considered.

Case Study: The Reservoir X

Reservoir X is in the Gulf of Mexico. The reservoir is made up of a series of turbidite sands of Miocene to Pliocene age deposited within a mini-basin. The reservoir was a good candidate for secondary recovery because it has limited aquifer influx, very over-pressured and compacting, with an initial reservoir pressure of 11,305 psia and was under saturated. The reservoir also has good structure relief, good connectivity and directional permeabilities. Its sands are generally characterized as sheet sands and channelized deposits but massive fine and very-fine grained sands are also observed. The sheets have excellent lateral pressure communication and shales at the

[9]Spath J. and McCants S. (1997), Waterflood Optimization using a Combined Geostatistical – 3D Streamline Simulation Approach: A Field Example. Paper 38355-MS presented at the SPE Rocky Mountain Regional Meeting, Wyoming, 18–21 May.

internal zones do not necessarily divide the reservoir into compartments as seen from production and pressure history.

As discussed by Lach[10], seawater injection commenced in 1999 when reservoir pressure was about 6,800 psia, approximately 4,500 psi below the original 11,305 psia and significant water break-through has occurred. Some of the waterflood objectives are to maintain/stabilize pressure to prevent the sands from producing below their bubble points and to minimize well completion. Its original oil in place is estimated at 534 MMSTB.

Table 1: Average properties of the Reservoir X (Lach[10])

PROPERTY	VALUE
Area (Acre)	4917
Average porosity, ø (%)	28
Average Water Saturation, S_{wa} (%)	0.22
Net/gross sand	0.9
Average Permeability, (mD)	125
Reservoir thickness, (ft)	99
Datum depth (ft)	16726
Initial reservoir pressure at datum, P_R (psi)	11305
Bubble point pressure (psia)	6306
Oil viscosity, μ (cP)	0.782
Oil initial FVF (rb/stb)	1.39

Reservoir Characterization and Static Reservoir Modeling

Stanford Geostatistical Modeling Software (SGEMS), an open-source computer package for solving problems involving spatially related variables, was used. Each reservoir property data was assessed using histograms and variograms. For each property, anisotropic variograms were used to adequately capture the spatial correlation between data points. The properties evaluated include: shale volume, lithofacies, total porosity, permeability, and net-to-gross ratio.

Statistical Analysis

Facies Interpretation

Reservoir X consists of deepwater turbidite sands and shale. There are three lithofacies of interest as seen from type logs shown in Figure 1. They include clean turbidite sandstone with a minor fraction of concretions, sandstone with significant concretions mixed with shale, and clearly non-reservoir facies consisting of shale and entirely cemented sandstone with representative codes of 1, 2 and 3 respectively. The spatial distribution of these facies types affects fluid flow tremendously.

[10]Lach J., IOR for Deepwater Gulf of Mexico: Phase 1, Knowledge Reservoir, Houston, Texas. 2010

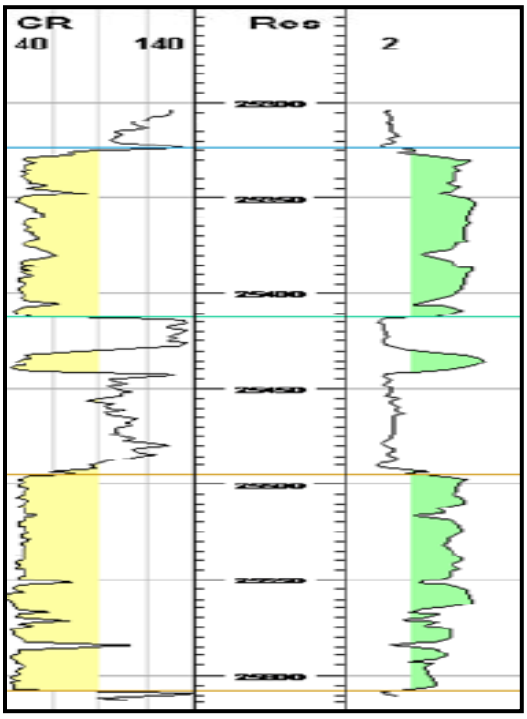

Figure 1: Type log of a well in the Reservoir X used to illustrate facies type (Lach[10]).

From the histogram plot (Figure 2), a unimodal distribution was observed with clean sandstone (facies 1) being the most common lithofacies in the reservoir. Also evident is the reservoir zone of interest with a significant proportion of sandstone with significant concretions mixed with shale (facies 2). To model the spatial correlation between the data points, anisotropic variograms were used in the variogram analysis. These models were to be used in the generation of lithofacies realizations.

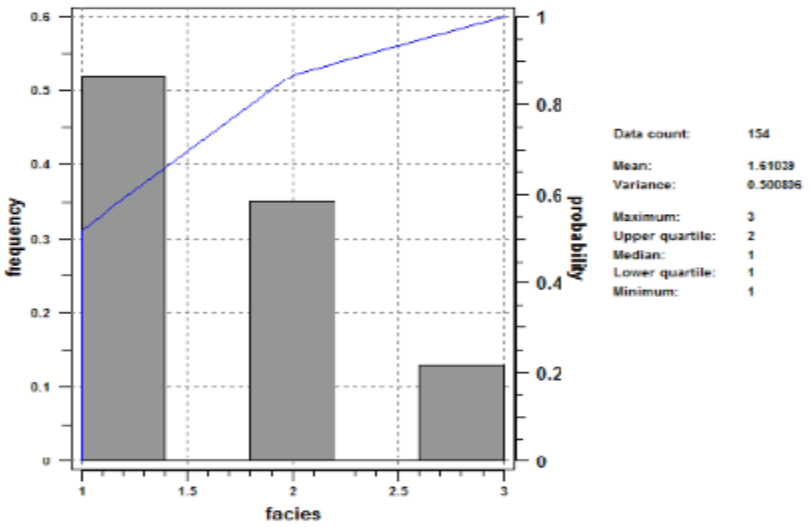

Figure 2: Histogram for lithofacies.

Porosity

From the histogram for porosity shown in Figure 3, a unimodal porosity distribution is observed with the minimum and maximum porosity values of 0.07 (6.96%) and 0.385 (38.5%) respectively.

The modal porosity values are between 0.25 and 0.26. The mean porosity value is 0.24 (24.3%) and the standard deviation is 0.06 (6.5%).

To aid in the generation of equiprobable realizations, variogram analysis was conducted on the porosity data set and Gaussian model was also used to fit the data set by visual inspection and the variogram directions captured the spatial variation in the porosity data points. However, due to the sparseness of the data points used in the model, it was necessary to generate cross variograms for porosity as the primary variable and shale volume, V_{sh}, as the secondary variable. The anisotropic and cross variograms generated were then used to build equiprobable realizations of the porosity for the model.

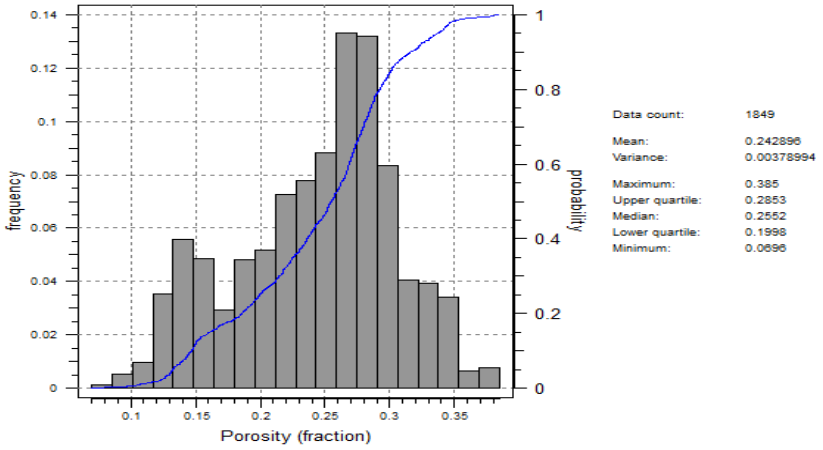

Figure 3: Histogram for porosity.

Permeability

Figure 4 is a plot of the histogram of the permeability data. A unimodal distribution was observed with the data range of 10 – 100 md (logperm values of 1-2) as the most likely. The average permeability is 1.92 (83.1 md) and the standard deviation is 1.87 (73.79 md). The range of log perm values was between -4.05 (0.0001md) and 3.43 (2700 md).

A variogram were then built to capture the spatial variation of permeability between data points. This variogram in combination with the anisotropic variogram earlier generated for porosity was then used in the building of equiprobable realizations of the permeability distribution across the model using sequential Gaussian co-simulation (COSGSIM). This was due to the sparseness of the data points used in the model. Hence a cross variogram for permeability as the primary variable and porosity as the secondary variable was built.

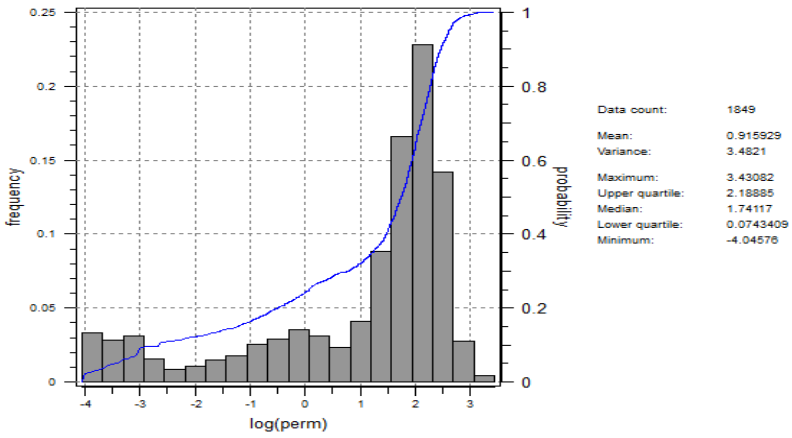

Figure 4: Histogram for permeability.

Net-to-Gross

As seen from the Figure 5, the NTG values peaked at 97.4% with the lowest value occurring at 55.4%. From the histogram plot, a unimodal distribution was observed. It was also observed that the most common or likely NTG value is around 55%. The mean value is 76.03% while a standard deviation of 19.6% was observed.

To model the spatial correlation between the data points, anisotropic and cross-variograms were built and were used to generate realizations. Also, it was necessary to generate cross variograms for net-to-gross as the primary variable and porosity as the secondary variable due to the sparseness of the data points used in the model.

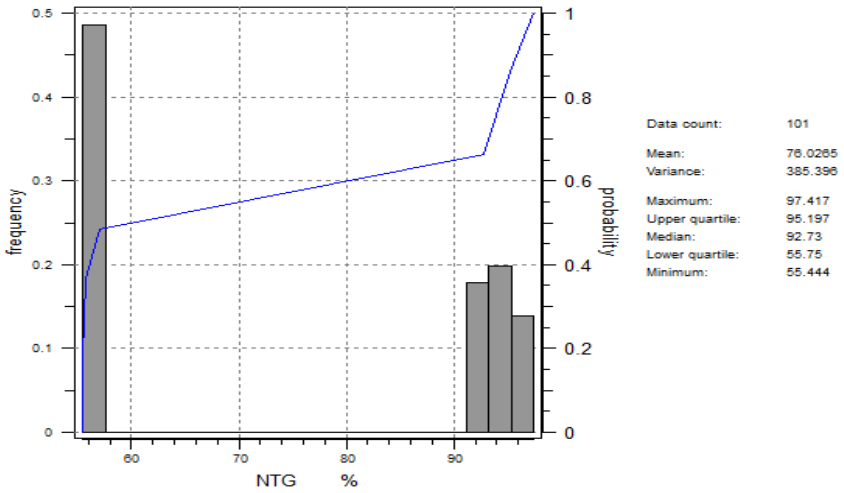

Figure 5: Histogram for net-to-gross ratio.

Shale Volume

Figure 6 is a histogram of the shale volume data. A unimodal distribution of shale volume was observed with the minimum and maximum values for NTG as 0 % and 99.6% respectively. It was also observed that the most common or likely shale volume value for the wells considered was within the rangeof 0 - 6%. This means that the reservoir contains a large amount of clean sandstone as observed from the facies histogram). The mean value is given as 17.3%. To model the spatial

correlation between the data points, an anisotropic variogram was generated for use in ~~the~~ realization generation.

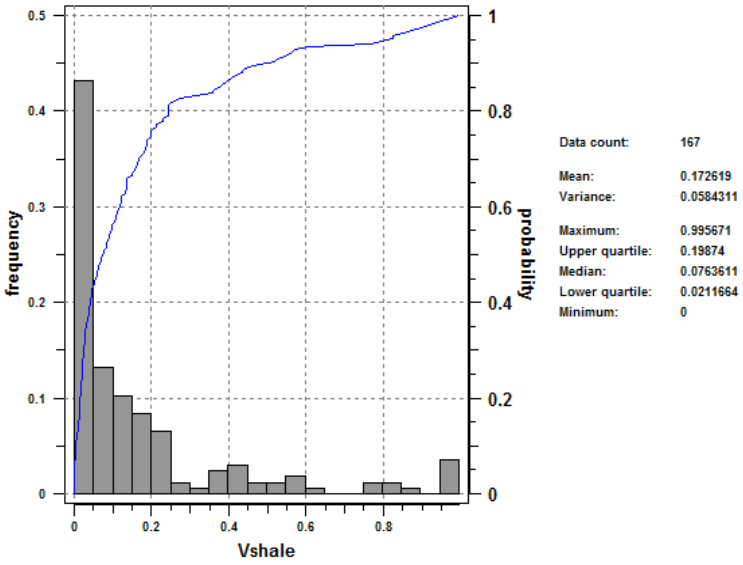

Figure 6: Histogram for shale volume.

Geostatistical Modeling of Reservoir Properties

To statistically estimate the reservoir properties over the entire volume of the Reservoir X model, simulation was used. Stochastic simulation was used instead of kriging so as to make it possible for the generation of multiple equiprobable realizations of the reservoir which allows for assessment of uncertainty. Table 2 shows a summary of the grid data used.

Table 2: Summary of grid data used in static modeling

Cell Dimensions (in feet)	
Length	400
Width	400
Thickness	20
Number of Cells in the X-direction	20
Number of Cells in the Y-direction	20
Number of Cells in the Z-direction	5
Total Number of Cells	2000

Facies Modeling

According to Chang[11], numerous methods exist for building facies models. These methods can be used to:

- Measure and define facies and facies models.
- Transfer geological information into digital data to quantify geological facies and facies models.

A reservoir characterization study was undertaken to model the facies distribution for the individual layers in the model using sample well logs, an example of which is shown in Figure 1. The Sequential Gaussian Simulation (SGSIM) was used to generate these distributions. The lithofacies distribution across the model is shown in Figure A1.

Petrophysical Modeling

Sequential Gaussian co-simulation (COSGSIM) was used to generate five realizations of each reservoir property accessed. The parameters obtained from the variogram analysis were used in this exercise. For each property, a maximum conditioning data of 12 was used with a seed value of 14071789. Due to the sparseness of data points in the model, co-simulation was performed on these reservoir properties. These properties are porosity and shale volume, permeability and porosity, and finally net-to-gross and porosity. As discussed by Remy[12], the sequential Gaussian co-simulation algorithm allows us to simulate a Gaussian variable (such as porosity and permeability) while accounting for the secondary information (such as shale volume). Figures A2 – A4 show the simulation maps for permeability, porosity and net-to-gross ratio respectively.

Ranking of Static Reservoir Models Built

Five static equiprobable descriptions of each reservoir property were generated using SGEMS. Table 3 shows the results of the statistical means obtained from the realizations maps generated for porosity, absolute permeability, and net-to-gross while comparing them with the means of the properties before static simulation.

Generally, the mean values after simulation of the petrophysical properties are slightly smaller than those of the raw data. This observation may be because of the variogram parameters employed for each property. Also, the variation in the maximum and minimum average values (Table 3) suggests the extremely high and low cases of what the reservoir static model could be. Thus, the third realizations of the models of porosity, permeability and net-to-gross were used in the waterflood simulation studies.

[11] Chang Li, (2010) Integration of Facies Models in Reservoir Simulation, Master's Thesis, The University of Texas at Austin.

[12]Remy N., Boucher A. and Wu J. (2009), Applied Geostatistics with SGEMS, Cambridge University Press, Cambridge

Table 3: Summary of the statistical means before and after building realizations

PROPERTY	BEFORE COSGSIM		AFTER COSGSIM		Realn. No.
Porosity	Mean	0.24	Minimum mean	0.15	2
			Mean (for all real.)	0.19	
			Maximum mean	0.24	3
Permeability	Mean	1.92 (83.1mD)	Minimum mean	1.86 (65.3 mD)	5
			Mean (for all real.)	1.82 (66.5mD)	
			Maximum mean	1.889 (76.9mD)	3
Net to Gross	Mean	76.03%	Minimum mean	68.06%	4
			Mean (for all real.)	69.11%	
			Maximum mean	71.05%	3

Estimation of Parameters to be used for Analysis

In this study, the effects of two factors on the reservoir waterflood performance will be analyzed. These factors are kV/kH ratio and Dykstra-Parsons Coefficient, and they quantify reservoir heterogeneity. Permeability distributions in the reservoir model were created to incorporate a range of these parameters.

Horizontal and vertical permeabilities

Permeability distributions across the reservoir model were created using geostatistical methods earlier described. Lognormal distributions were used to represent permeabilities. These permeability values are taken as the average permeability, k_{avg}, such that:

$$k_{avg} = \sqrt[3]{k_X . k_Y . k_Z} \quad \text{---------- 1}$$

Then, using a range of kV/kH ratios, for instance 0.05, 0.20, 0.40, etc., it is derived that

$$k_{avg} = k_H . \sqrt[3]{x} \quad \text{---------- 2}$$

where x = 0.05, 0.20, 0.40, etc.

The derivation of equation 2 is shown in Appendix B.

To obtain directional permeabilities, an assumption that permeability in the y-direction is 80% of the permeability in the x-direction was made[9]. Hence, horizontal permeability, k_H, is calculated as:

$$k_H = \sqrt{k_X \, . k_Y} \text{ ---------- 3}$$

Finally, permeability in the z – direction is calculated from equation 2 as:

$$k_z = k_V = \frac{(k_{avg})^3}{k_X \, . k_Y} \text{ ---------- 4}$$

Reservoir Heterogeneity (Dykstra-Parsons Coefficient)

To predict and interpret the displacement of reservoir of fluids during a waterflood operation, it is important to:

- describe the degree of the vertical heterogeneity in mathematical terms.
- describe and define the proper permeability stratification of the pay zone (layering problem).

The Dykstra-Parsons permeability variation coefficient V and the Lorenz coefficient L are the most widely used parameters in describing the vertical heterogeneity of a formation. The Lorenz coefficient is limited in that it is not a unique measure of reservoir non-uniformity.

The Dykstra-Parsons permeability variation was introduced in 1950. Generally, it is a statistical measure of non-uniformity of a set of data. It is generally applied to the property of permeability but can be extended to treat other rock properties. It characterizes the distribution of permeability around the geometric mean. The required computational procedures for determining the coefficient V_{DP} are summarized below:

Step 1: Arrange the core samples in decreasing permeability sequence, i.e. in descending order.

Step 2: For each permeability value, get the rank data index, j.

Step 3: Calculate the cumulative probability distribution, j/(N+1).

Step 4: Calculate the probability density function, z.

Step 5: Plot z-values versus permeability

Step6: Read the corresponding permeability values at z =1 and z = 0. These are the permeability values at 84.1% and 50% of thickness respectively and they are designated as $k_{84.1}$ and k_{50}.

Step 7: The Dykstra-Parsons permeability variation is defined by the following expression:

$$V = \frac{k_{50} - k_{84.1}}{k_{50}} \text{ ---------- 5}$$

Reservoir Simulation and Waterflood Performance Analysis

Reservoir Simulation Model Initialization

The reservoir X model is an under saturated reservoir with an initial average reservoir pressure of 11305 psia. The oil initially in place (OIIP) after initialization is put at 1.792 MMSTB. The other properties of the reservoir are stated in sections 3.4 and 3.5. The reservoir model is five (5) layered, with 2000 grid cells out of which 1410 cells are active grid cells. The effects of gravity segregation as well as fluid and rock compressibilities were included in the simulation runs of the model. The start time for the simulation is June 1, 1996.

Waterflooding of the Reservoir X

Reservoir Development Plan

The production scheme used for this reservoir model involved two stages. Firstly, the development of the field began in June 2004, with just one producer with oil flow rate of 1000 STB/day. Upon production, it was decided that waterflooding should be commenced after three (3) years of production and it was carried out for ten (10) years.

Waterflooding was carried out to increase and/or maintain reservoir pressure above bubble point (6306 psia) and increase the oil producing rate of the field. Waterflooding started in June 1999 with four (4) injectors for each of the scenarios, all injecting at a rate of 700 STB of water/day. The injectors were positioned such that the waterflood pattern approximated the regular five-spot. Water was injected into the aquifer zone (zone 5) and the producers were completed in zones 2 – 4.

These rates were used throughout the period of simulation. The economic limit for producers consists of 50 STB/day for production rate and a maximum water-cut of 0.95. This production strategy was used for analysis of the effects of kV/kH ratio and reservoir heterogeneity on waterflooding. Comparisons of waterflood performance were based on field average reservoir pressure (FPR), cumulative oil production (FOPT), and field water-cut (FWCT) for a period of thirteen (13) years (8 years of primary depletion and 5 years of waterflooding).

Methodology for Analyzing the Effect of kV/kH Ratio (kV/kH) on Waterflood Performance

Four kV/kH ratios were selected and their effect on the waterflood performance analyzed. They are:

- k_V/k_H ratio of 0.001 **(kVkH_0.001),**
- k_V/k_H ratio of 0.01**(kVkH_0.01),**
- k_V/k_H ratio of 0.10**(kVkH_0.1),** and
- k_V/k_H ratio of 0.60**(kVkH_0.60).**

The base case of the kV/kH ratios is 0.6.

Methodology for Analyzing Effect of Reservoir Heterogeneity (Dysktra-Parsons Coefficient, V_{DP}) on Waterflood Performance

The Dysktra-Parsons Coefficient, abbreviated as V_{DP} in this study, was used as a measure of the heterogeneity of the reservoir. For the base case of kV/kH ratios, kV/kH = 0.60, five Dysktra-Parsons Coefficients (**V_{DP}**) were chosen. They are:

- Dysktra-Parsons Coefficient of 0.40 (**VDP_0.4**),
- Dysktra-Parsons Coefficient of 0.50 (**VDP_0.5**),
- Dysktra-Parsons Coefficient of 0.70 (**VDP_0.7**), and
- Dysktra-Parsons Coefficient of 0.90 (**VDP_0.9**).

The base case of Dysktra-Parsons coefficients is 0.70.

RESULTS AND DISCUSSION

Analysis of Waterflood Performance

In this section, the results obtained from the waterflooding of the Reservoir X are presented and analyzed. The results showing effect of kV/kH ratios on waterflood performance are compared and discussed first, followed by those on the effects of reservoir heterogeneity.

Effect of kV/kH Ratios on Waterflood Performance

The presented pattern scenario is the regular five-spot pattern.

Effect of kV/kH Ratios on the Field Oil Producing Rate (FOPR)

Figure 7 is a plot of oil producing rate of the field vs. time for a five-spot waterflood considering four kV/kH ratios – 0.001, 0.01, 0.1 and 0.6. Simulation was carried out for thirteen (13) years – three (3) years of primary production and ten (10) years of waterflood. As earlier stated, the total production rate from the wells was fixed at 1000 stb/day and the total injection rate at 2800 stb/day (700 stb/day for each injector) for all scenarios.

Generally, it was seen that cases with lower kV/kH ratios had lower oil production rate when compared to cases with higher kV/kH ratios. This is because for reservoirs with low vertical-to-horizontal permeability ratios, there is poor reservoir fluid transmissibility in the vertical direction from one zone to another. This results in poor mobility/sweep efficiency of the injected water and hence lowers oil production rates.

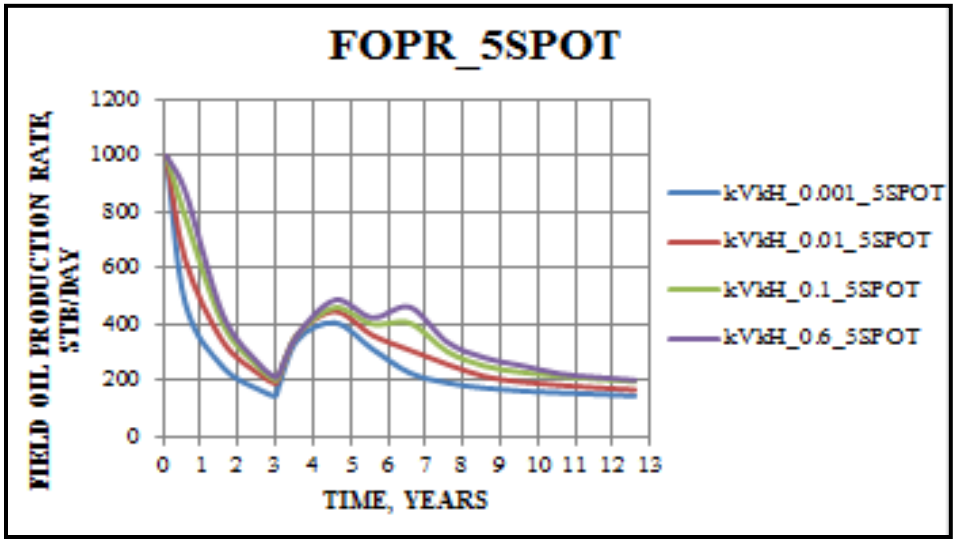

Figure 7: Plot of field oil production rate vs. time for different k_V/k_H ratios.

However, cases with higher kV/kH ratios show higher oil production rate compared to cases with lower kV/kH ratios due to good vertical transmissibility between layers due to good communication between zones in the reservoir.

Figures 8 - 11 are maps showing the distribution of oil saturation across zone 3 of the Reservoir X at the end of simulation (01/01/2009) for all kV/kH cases analyzed – Cases KVKH 0.001, 0.01, 0.1, 0.6. It is clearly observed that for cases KVKH 0.001 and 0.01, the oil saturation in cells around the producers was very low (very close to zero). This was because, for these cases, there was limited crossflow/transmission of oil from neighboring zones in the vertical and horizontal

directions. Hence there was poor replenishment of already depleted reservoir zones by oil from neighboring zones throughout the period of simulation.

However, for cases with good kV/kH ratio (Cases KVKH 0.001 and 0.01), the oil saturations in cells around the production wells are between the ranges of 0.11 – 0.55 even at the end of simulation (a period of oil withdrawal from those zones). This is because there is better flow of oil in the horizontal and vertical directions from neighboring zones to replenish already depleted zones.

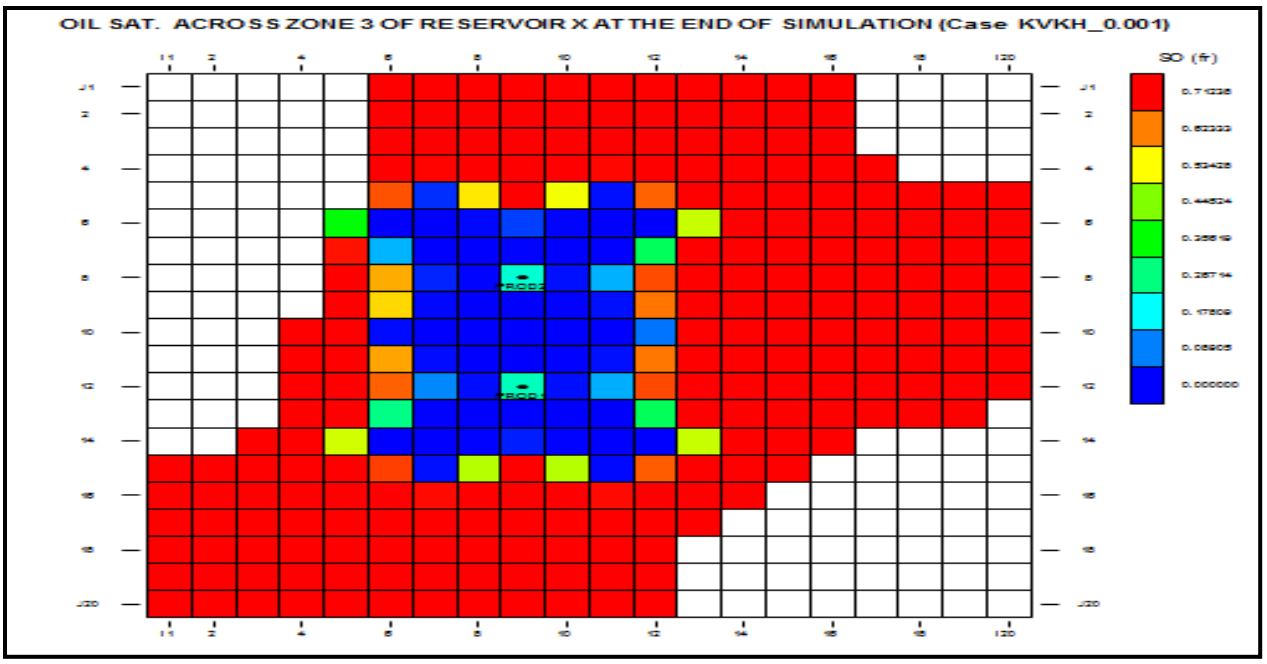

Figure 8: Map showing the distribution of oil saturation across zone 3 of the Reservoir X and the location of producers at the end of simulation (01/01/2009) for kV/kH case KVKH_0.001.

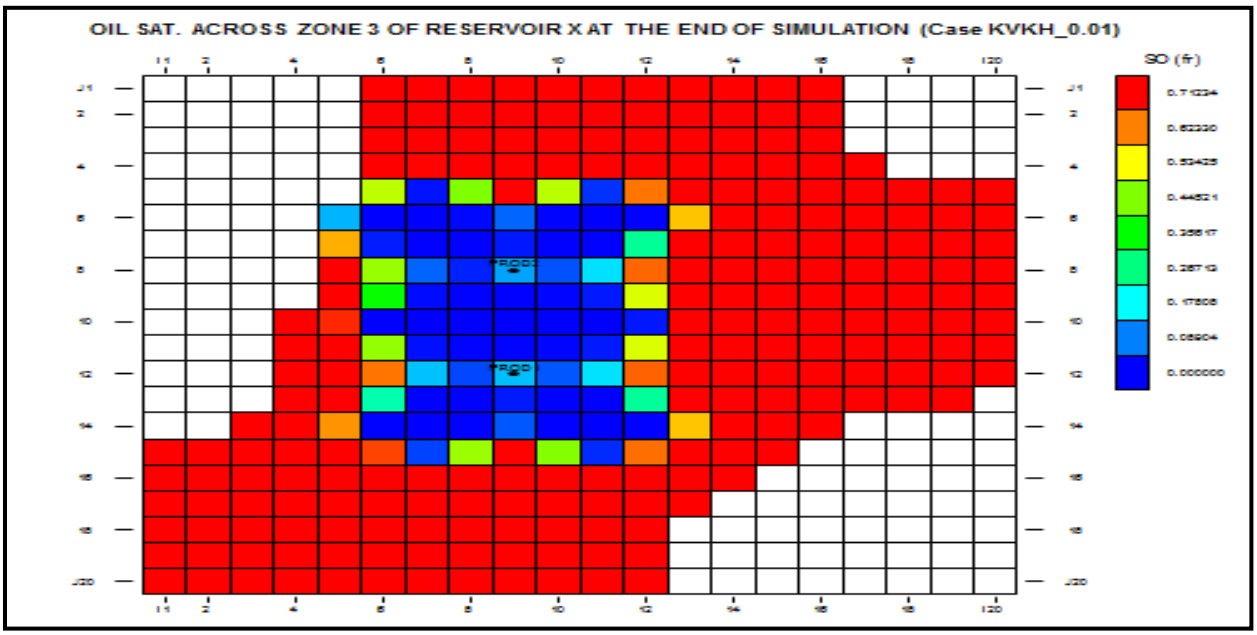

Figure 9: Map showing the distribution of oil saturation across zone 3 of the Reservoir X and the location of producers at the end of simulation (01/01/2009) for kV/kH case KVKH_0.01.

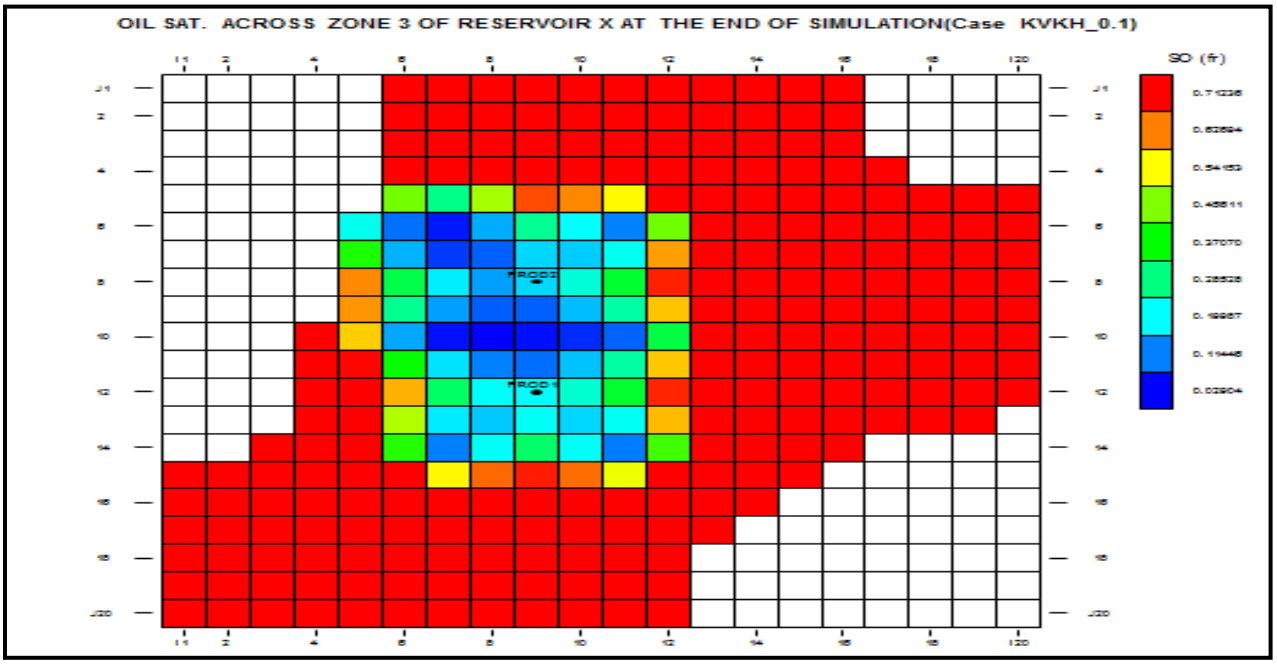

Figure 10: Map showing the distribution of oil saturation across zone 3 of the Reservoir X and the location of producers at the end of simulation (01/01/2009) for kV/kH case KVKH_0.1.

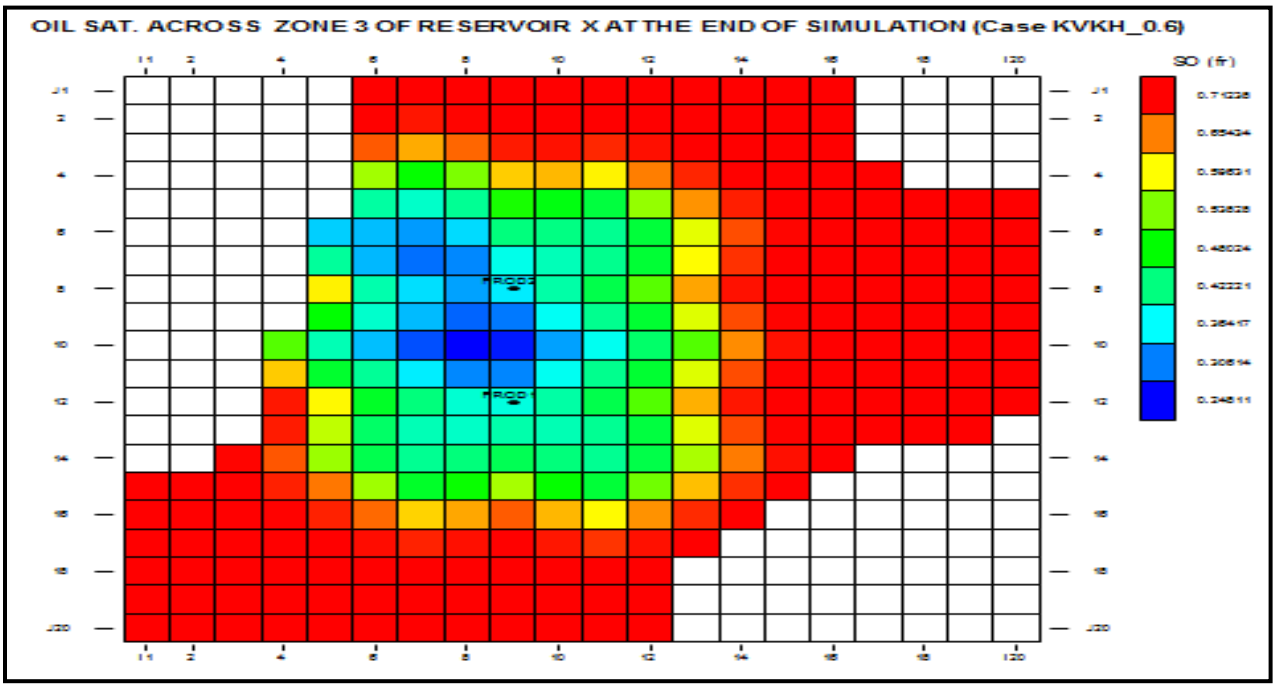

Figure 11: Map showing the distribution of oil saturation across zone 3 of the Reservoir X and the location of producers at the end of simulation (01/01/2009) for kV/kH case KVKH_0.6.

Effect of kV/kH Ratios on Cumulative Oil Production (FOPT)

Figure 12 is a plot of cumulative oil production vs. time for the five-spot waterflood considering four kV/kH ratios – 0.001, 0.01, 0.1 and 0.6. Note that waterflood for each kV/kH ratio was simulated for ten (10) years. The results show that cumulative oil production improves with increasing kV/kH ratio (with approximately 300 MSTB, 360 MSTB, 405 MSTB and 425 MSTB for the kV/kH ratio scenarios of 0.001, 0.01, 0.1 and 0.6 respectively). This is because the sweep efficiency of the waterflood improves with better kV/kH ratios. This is due to improved crossflow/fluid transmissibility between layers from non-depleted zones to already depleted zones within the reservoir. Better sweep efficiency could also lead to lower water-cut which was observed for these cases at the end of simulation.

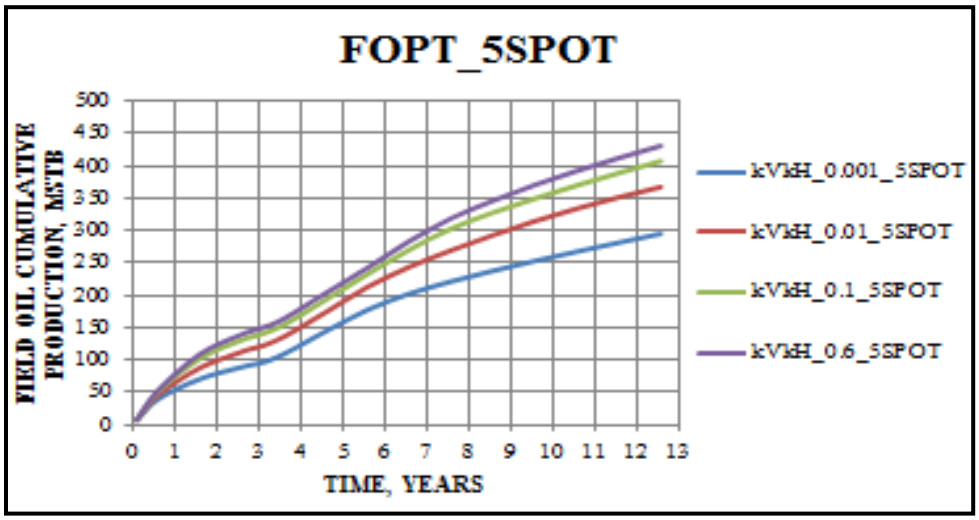

Figure 12: Plot of field cumulative oil production vs. time for different k_V/k_H ratios.

Effect of kV/kH Ratios on Reservoir Pressure (FPR)

Figure 13 is a plot of average reservoir pressure of the Reservoir X vs. time for the five-spot waterflood considering four kV/kH ratios – 0.001, 0.01, 0.1 and 0.6. Waterflood for each kV/kH ratio was simulated for ten (10) years. From the figure, it is observed that higher kV/kH ratios showed lower pressure decline. Case kVkH_0.60 has the lowest pressure decline while Case kVkH_0.001 has the highest pressure decline throughout the period of simulation. This can be attributed to the fact that there is little communication between the zones for reservoirs with low kV/kH ratios and hence lower pressure maintenance. Recall that injected water moves preferentially in the vertical upward direction due to gravity. A high kV/kH ratio implies good vertical communication between reservoir zones and hence easier movement of injection water vertically. This results in better pressure maintenance. Also, the injected water would flow into non-injected zones, thus improving pressure maintenance.

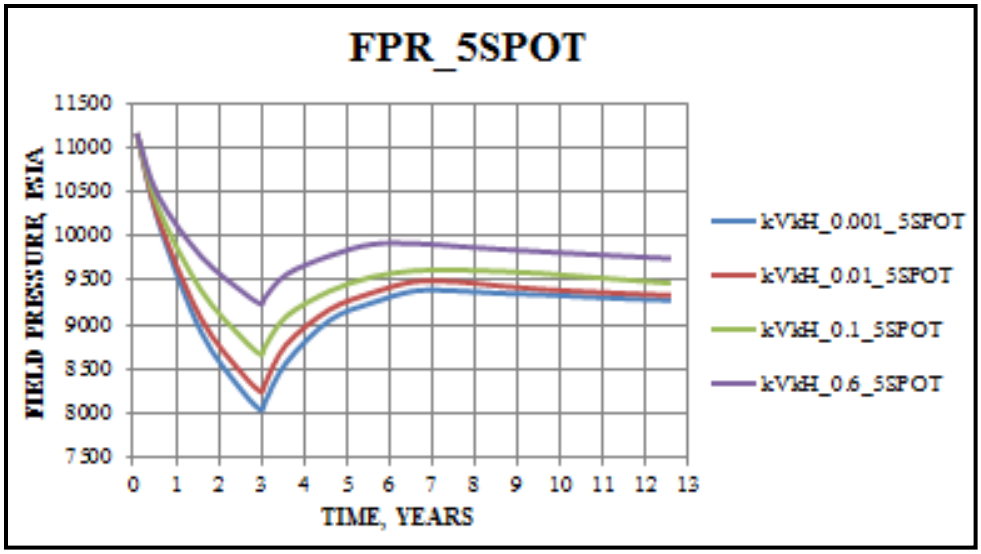

Figure 13: Plot of field pressure vs. time for different k_V/k_H ratios.

Effect of kV/kH Ratios on Field Water-Cut (FWCT)

Figure 14 shows a plot of field water-cut vs. time of all the kV/kH cases studied for the five-spot. It is seen that for all scenarios analyzed, all kV/kH cases showed no significant water breakthrough prior to waterflooding until around five (5) years of production. The trend of field water-cut for all the scenarios of waterflood considered is observed to be like the highest water-cut of less than 80% at the end of simulation. This is because the number of injectors and injection rate for each scenario are the same.

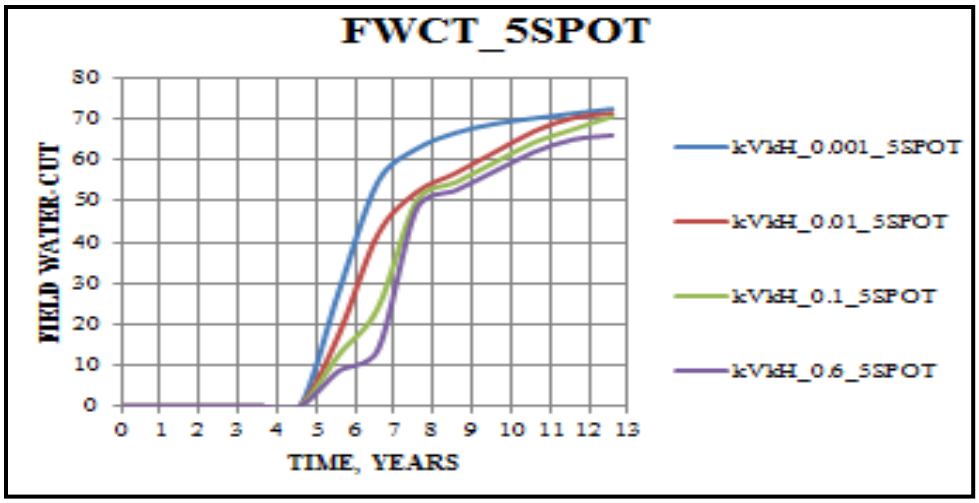

Figure 14: Plot of field water-cut vs. time for different k_V/k_H ratios.

Also observed is that for all scenarios, increasing kV/kH ratios lead to higher water-cut. This is because the sweep efficiency in all zones improves with increasing kV/kH ratios, since there is increased communication between the zones. This can substantially increase water production at the producers and subsequently, field water-cut. For cases of very low kV/kH ratios (kVkH_0.001 and kVkH_0.01), there is poor communication between zones and hence, lower water production.

Effect of Reservoir Heterogeneity on Waterflood Performance

Under this section, the impact of reservoir heterogeneity (measured using the Dykstra-Parsons coefficient) on waterflood is analyzed. Reservoir heterogeneity is based on distribution of permeabilities and V_{DP} and the kV/kH ratio for all cases considered was set at 0.60. From results obtained, it was seen that the waterflood scheme performed better based on degree of heterogeneity. This shows that reservoir heterogeneity plays a vital role in waterflood performance. The waterflood pattern employed was the five-spot pattern.

Effect of Reservoir Heterogeneity on Oil Production Rate (FOPR)

Figure 15 is a plot of field oil production rate vs. time for all cases of reservoir heterogeneity studied. The plots show that cases with lower coefficients of heterogeneity (VDP_0.4 and VDP_0.5) have higher oil rate throughout the simulation period than for cases with higher heterogeneity. Generally, it is observed that the more heterogeneous the reservoir is, the lower the oil production rate with time when compared to reservoirs which are less heterogeneous. This is because factors that contribute to reservoir heterogeneity such as variation in permeability and porosity within the reservoir sands caused mainly by presence of shale and cemented sandstones result in poor horizontal and vertical sweep and hence a substantial amount of oil is bypassed by the injected water. Reservoirs which are less heterogeneous tend to show better injectivity and productivity than reservoirs which have a higher degree of heterogeneity. This is because for these reservoirs, for a given level of good horizontal and vertical cross–flow between reservoirs layers and zones which allow replenishment of depleted zones by neighboring zones, the injected and produced fluids flow easily through pore spaces due to lack of flow barriers caused by presence of shale and cemented sandstones.

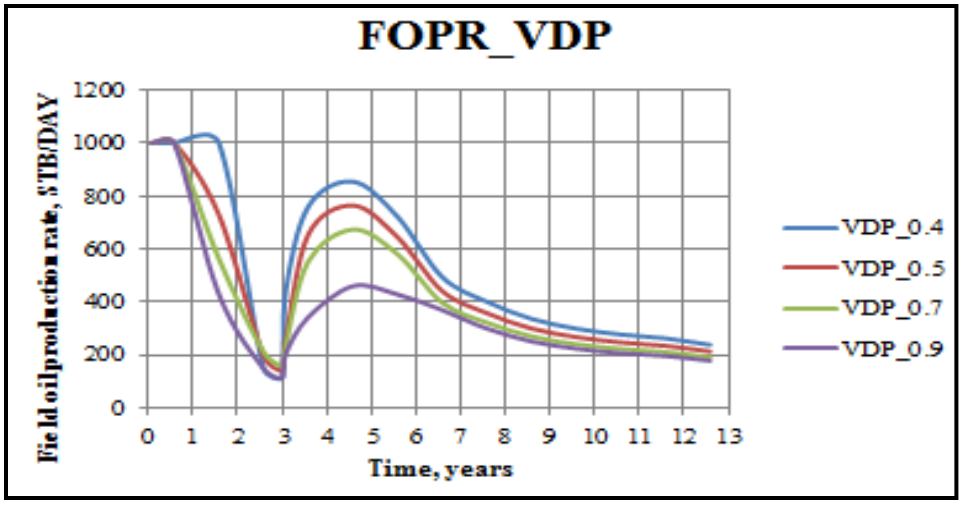

Figure 15: Plot of field oil production rate vs. time for different V_{DP} scenarios.

Effect of Reservoir Heterogeneity on Field Water-Cut (FWCT)

Figure 16 is a plot of field water-cut vs. time for all cases of reservoir heterogeneity studied. From the plot, it is observed that the field water-cut decreases significantly with increasing heterogeneity after waterflooding. This is because, with increase in reservoir heterogeneity, there is poorer displacement efficiency of reservoir fluids. This can result in reduced water production as observed for cases with higher heterogeneity (VDP_0.7 and VDP_0.9).

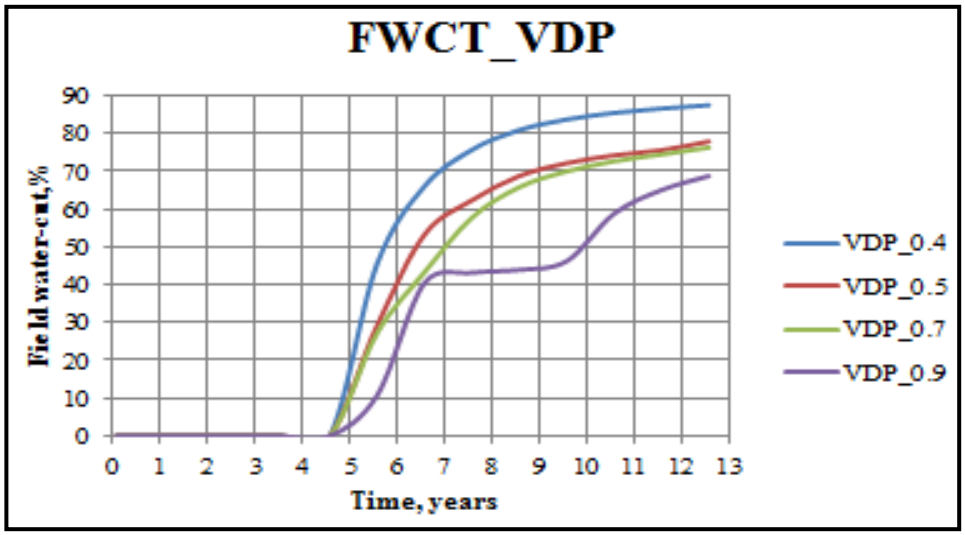

Figure 16: Plot of field water-cut vs. time for different V_{DP} scenarios.

For scenarios with lower coefficient of heterogeneity (VDP_0.4 and VDP_0.5), it is observed that the general trend in field water-cut throughout the period of simulation is higher in comparison to cases with higher heterogeneity. This is because injected water flows easily through the pore spaces of reservoirs with lesser degree of heterogeneity. In such reservoirs, there is lack of flow barriers caused by presence of shale and cemented sandstones across the reservoir rocks, thus resulting in better movement of injected water. This could also lead to higher water-cut as injected water flows quite easily to the producers.

Effect of Reservoir Heterogeneity on Cumulative Oil Production (FOPT)

Figure 17 is a plot of Reservoir X cumulative production vs. time for the V_{DP} scenarios analyzed – 0.4, 0.5, 0.7, and 0.9. All scenarios analyzed show that cumulative oil production decreases with increasing reservoir heterogeneity. Factors that contribute to reservoir heterogeneity, such as variations in permeability and porosity within the reservoir sands caused mainly by presence of shale and cemented sandstones, can cause poor movement of reservoir oil/gas and injected water.

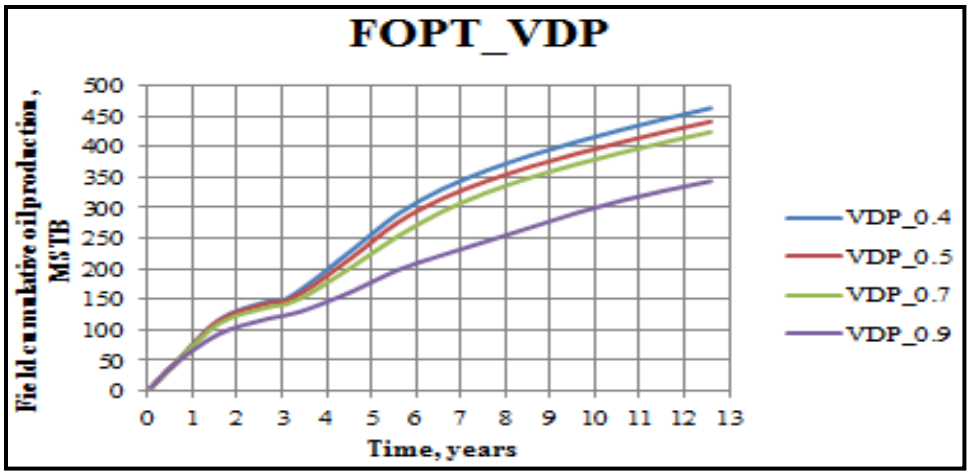

Figure 17: Plot of field cumulative production vs. time for all V_{DP} scenarios.

Prior to waterflooding, it was observed that cases VDP_0.4, VDP_0.5 and VDP_0.7 (cases with lesser reservoir heterogeneity) had similar cumulative oil recovery than case VDP_0.9. This is

because reservoir fluids move easily through pore spaces of less heterogeneous reservoirs than those of more heterogeneous reservoirs. Also upon waterflooding after 3 years of primary production, it was observed that cumulative oil production also decreased with increasing reservoir heterogeneity. This is because displacement efficiency of oil by the injected water decreased with increasing reservoir heterogeneity. This resulted in bypassed oil and thus lower cumulative oil production with time.

Reservoirs which are less heterogeneous tend to better injectivity and productivity than reservoirs with a higher degree of heterogeneity. This is because for these reservoirs, for a given level of good horizontal and vertical cross–flow between reservoir layers and zones which allow replenishment of depleted zones by neighboring zones, the injected and produced fluid flow easily through pore spaces due to absence of flow barriers caused by presence of shale and cemented sandstones.

Effect of Reservoir Heterogeneity on Reservoir Pressure (FPR)

Figure 18 is a plot of average reservoir pressure of Reservoir X vs. time for the V_{DP} scenarios analyzed – 0.4, 0.5, 0.7, and 0.9. Note that waterflood for each V_{DP} scenario was simulated for ten (10) years after three (3) years of primary production. It should also be noted that reservoir pressure in any waterflood operation is a function of voidage replacement of already produced fluids by injected water.

It is clearly seen that the profile of average reservoir pressure, FPR, is better maintained with decreasing reservoir heterogeneity. This is due to the presence of barriers to fluid flow in reservoirs with higher degree of heterogeneity, resulting in poor voidage replacement. Hence, reservoirs with lesser degree of heterogeneity have better pressure maintenance/increase due to easier movement of injected fluids within reservoir pore spaces, and hence better voidage replacement. These are all indicators of a good waterflood performance.

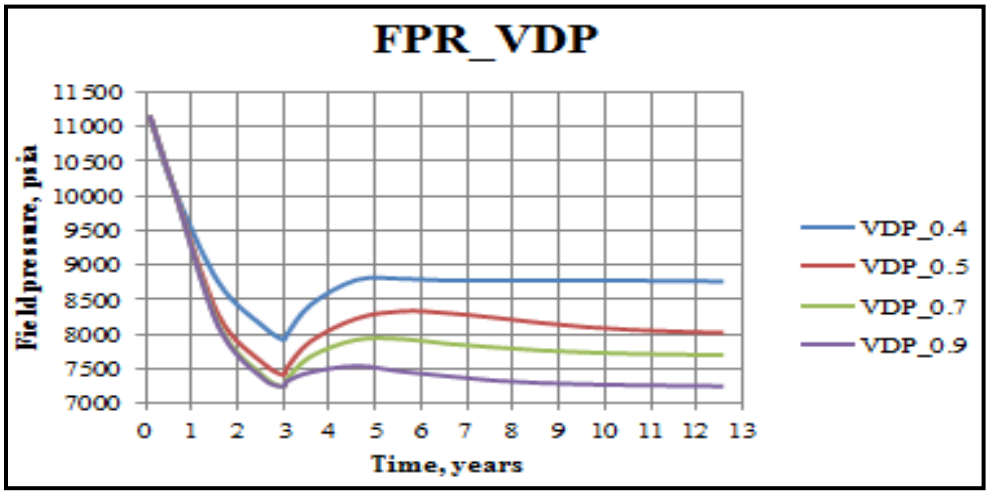

Figure 18: Plot of field pressure vs. time for different V_{DP} scenarios.

CONCLUSIONS

1. It is observed that permeability anisotropy affects waterflood performance. Lower kV/kH ratio across a reservoir implies less likelihood of vertical cross-flow between layers. In these cases, there is poor reservoir fluid transmissibility in the vertical direction from one zone to another. This results in poor mobility/sweep efficiency of the injected water, and hence lowers oil production rates. However, cases with higher kV/kH ratios show higher oil producing rate

compared to cases with lower kV/kH ratios due to good vertical transmissibility between layers because of good communication between zones in the reservoir.

2. For a reservoir with good kV/kH ratios, there is better pressure maintenance upon waterflooding. This is because injected water moves preferentially in the vertical upwards direction due to gravity. A high kV/kH ratio implies good vertical communication between reservoir zones and hence easier movement of injection water vertically.
3. Reservoir lateral and vertical heterogeneity affects injection and production from an oil-bearing system. The more heterogeneous a reservoir is, the more difficult it is to inject water and produce oil from it. This is because factors that contribute to reservoir heterogeneity, such as variation in permeability and porosity within the reservoir sands, caused mainly by presence of shale and cemented sandstones, result in poor horizontal and vertical sweep and hence the injected water bypasses much oil.

NOMENCLATURE

V_{DP} = Dykstra-Parsons Coefficient, dimensionless

BHP = Bottom-Hole Pressure, psia

FOPR = Field Oil Production Rate, STB/D

FOPT = Field Oil Production Total, STB

FWCT = Field Water-Cut, %

FPR = Field Pressure, psia.

APPENDIX

Appendix A

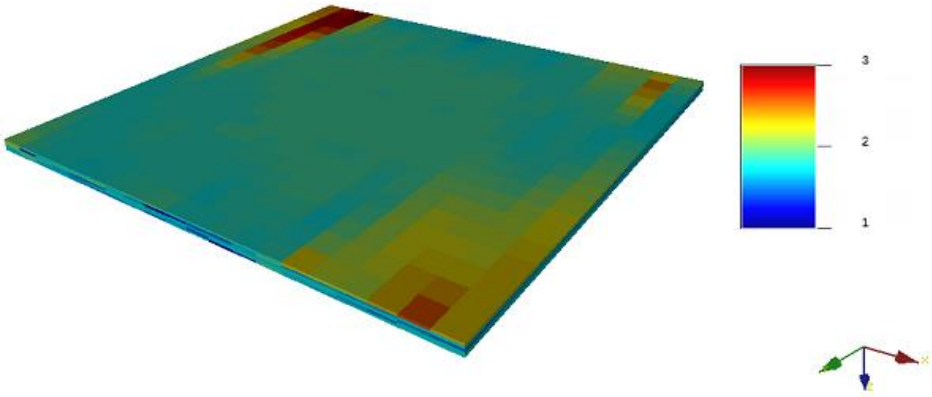

Figure A1: Simulation map of facies distribution across the Reservoir X model.

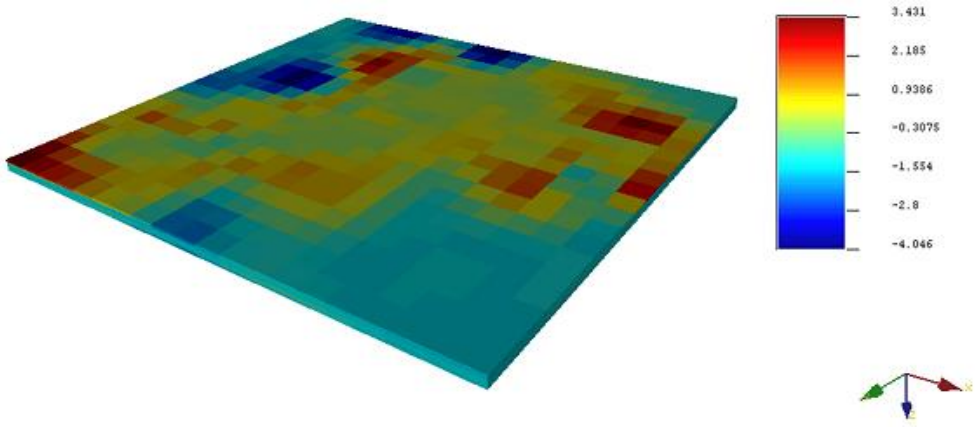

Figure A2: Simulation map showing permeability distribution across the Reservoir X model.

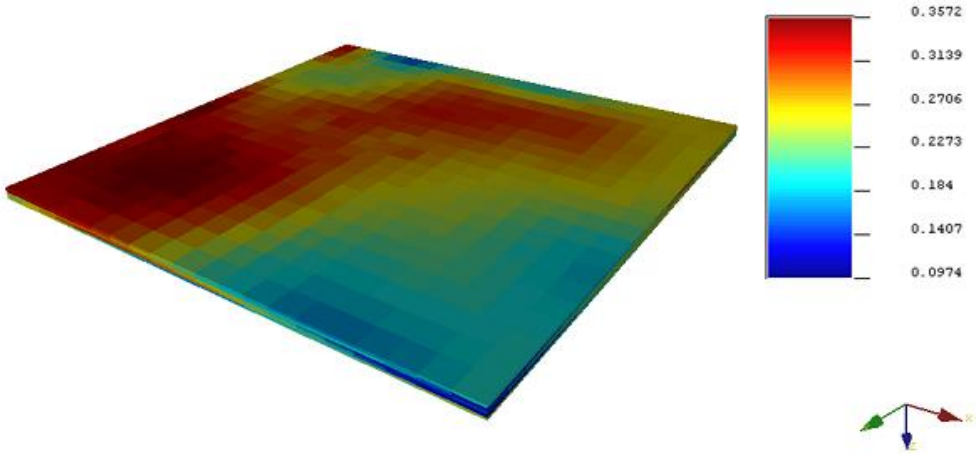

Figure A3: Simulation map showing porosity distribution across the Reservoir X model.

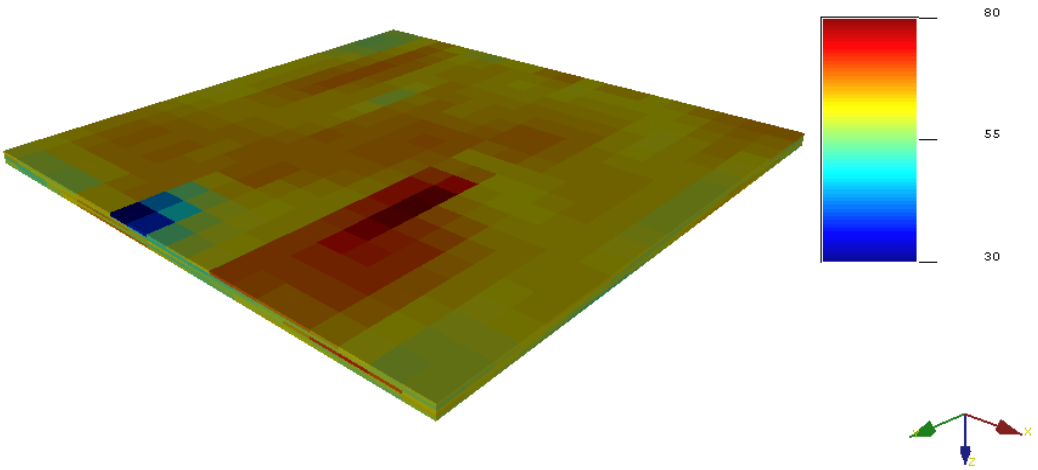

Figure A4: Simulation map showing net-to-gross distribution across the Reservoir X model.

Appendix B

This appendix presents the derivation of the equation used in estimating horizontal and vertical permeabilities (Equations 1 through 3).

Proof:

It is known that average permeability k_{avg} is given as:

$$k_{avg} = \sqrt[3]{k_X . k_Y . k_Z} \quad \text{---------- B.1}$$

Where k_x, k_y and k_z are the permeabilities in the x, y and z directions respectively.

Therefore,

$$k_{avg}{}^3 = k_X . k_Y . k_Z \quad \text{---------- B.2}$$

But, horizontal permeability, k_H is given as:

$$k_H = \sqrt{k_X . k_Y} \quad \text{---------- B.3}$$

Therefore,

$$k_H{}^2 = k_X . k_Y \quad \text{---------- B.4}$$

Equation B.2 therefore becomes:

$$k_{avg}{}^3 = k_H{}^2 . k_Z \quad \text{---------- B.5}$$

Using a range of kV/kH ratios, for instance 0.001, 0.01, 0.1 and 0.6, it is derived that

$$k_Z = k_H . x \quad \text{---------- B.6}$$

Where $k_V = k_Z$ and x = 0.001, 0.01, 0.1 or 0.6.

Combining equations B.5 and B.6, we have: that:

$$k_{avg}{}^3 = k_H{}^2 . k_H . x \quad \text{---------- B.7}$$

This means that:

$$k_{avg}{}^3 = k_H{}^3 . x \quad \text{---------- B.8}$$

Therefore

$$k_{avg} = k_H . \sqrt[3]{x} \quad \text{---------- B.9}$$

ACKNOWLEDGEMENTS

The authors would like to express profound appreciate to Mr. Brian Coats of Coat Engineering, Inc., USA for donating the SENSOR 6K simulator software used for this research, and to both Mr. Evans Boah Annah and Mr. Borsah Kofi Aidoo of African University of Science and Technology, Abuja, for the assistance they rendered.